HHS Public Access

Author manuscript

Proc SPIE Int Soc Opt Eng. Author manuscript; available in PMC 2024 June 21.

Published in final edited form as:

Proc SPIE Int Soc Opt Eng. 2024 February ; 12926: . doi:10.1117/12.3005223.

ASL MRI Denoising via Multi Channel Collaborative Low-Rank Regularization

Hangfan Liu,

Bo Li,

Yiran Li,

Rebecca Welsh,

Ze Wang

Center for Advanced Imaging Research, University of Maryland School of Medicine, Baltimore, MD, USA 21202

Abstract

Arterial spin labeling (ASL) perfusion MRI is the only non-invasive imaging technique for quantifying regional cerebral blood flow (CBF), which is a fundamental physiological variable. ASL MRI has a relatively low signal-to-noise-ratio (SNR). In this study, we proposed a novel ASL denoising method by simultaneously exploiting the inter- and intra-receive channel data correlations. MRI including ASL MRI data have been routinely acquired with multi-channel coils but current denoising methods are designed for denoising the coil-combined data. Indeed, the concurrently acquired multi-channel images differ only by coil sensitivity weighting and random noise, resulting in a strong low-rank structure of the stacked multi-channel data matrix. In our method, this matrix was formed by stacking the vectorized slices from different channels. Matrix rank was then approximately measured through the logarithm-determinant of the covariance matrix. Notably, our filtering technique is applied directly to complex data, avoiding the need to separate magnitude and phase or divide real and imaginary data, thereby ensuring minimal information loss. The degree of low-rank regularization is controlled based on the estimated noise level, striking a balance between noise removal and texture preservation. A noteworthy advantage of our framework is its freedom from parameter tuning, distinguishing it from most existing methods. Experimental results on real-world imaging data demonstrate the effectiveness of our proposed approach in significantly improving ASL perfusion quality. By effectively mitigating noise while preserving important textural information, our method showcases its potential for enhancing the utility and accuracy of ASL perfusion MRI, paving the way for improved neuroimaging studies and clinical diagnoses.

Keywords

Arterial spin labeling (ASL) MRI; denoising; low rank

1. INTRODUCTION

Arterial spin labeling (ASL) stands as a non-invasive and non-ionizing technique within perfusion MRI, facilitating the measurement of cerebral blood flow (CBF) [1–5]. Employing

radio-frequency pulses, ASL MRI tags the arterial blood water and captures perfusion-weighted MR images as this labeled arterial blood infiltrates the desired brain tissues. Over recent decades, ASL MRI has seen increasing applications across various clinical domains [6–10]. However, its comprehensive potential is curbed by the inherently low signal-to-noise ratio (SNR) in the perfusion effect, primarily due to T1 decay of the labeled arterial blood during post-labeling transit time. To address this challenge, the standard approach involves acquiring multiple label and control (L/C) image pairs and averaging their corresponding perfusion measurements. Yet, this method demands numerous L/C pairs to significantly boost SNR, impractical due to prolonged scan times and heightened motion risks. Moreover, averaging across multiple pairs may blur images due to inevitable subtle inter-frame movements.

In the realm of ASL denoising, initial methods relied on principal component decomposition-based noise removal [11], wavelet-domain filtering [12], or independent component decomposition-based noise suppression [13]. Later endeavors have expanded into spatio-temporal denoising frameworks, encompassing support vector machine-based CBF quantification and denoising algorithms [14] and total generalized variation regularization-based spatio-temporal filtering [15]. Meanwhile, Liang et al. fused nonlocal means [16] with dual-tree complex wavelet transform [17], and Xie et al. designed a deep convolutional neural network for ASL denoising [18], yielding enhanced outcomes. Nevertheless, these approaches overlooked the full utilization of multi-channel data to optimize performance, leaving their results less than satisfactory.

Consequently, the quest for advanced ASL denoising methods persists, aiming to surmount these challenges and unlock the technique’s full potential. Inspired by effectiveness of low-rank and sparse models for image denoising [19–27], this study attempts to enhance ASL MRI SNR by utilizing the low-rank property of the multi-channel data. Specifically, to preserve regional image contrast while suppressing the non-structural noise, we proposed a method that constructs a data matrix through stacking vectorized slices from different channels, and achieves denoising and texture preservation through an iterative optimization process which dynamically regularize the rank of the denoised data matrix to be low based on the estimated noise level. A notable advantage of our proposed framework is its independence from parameter tuning, setting it apart from existing methods. The efficacy of the approach is validated on real-world imaging data. The obtained experimental results convincingly demonstrate the significant enhancement in ASL perfusion quality. By addressing the limitations of current techniques, the ultimate goal of this study is to substantially improve the utility and accuracy of ASL perfusion MRI, leading to more reliable and informative neuroimaging studies and enhanced precision in clinical diagnoses.

2. METHOD

In our pursuit of maximizing information utilization for ASL denoising, we capitalize on the inherent low-rank structure within the multi-channel complex imaging data. Unlike conventional methods that use magnitude data after combining all channels, our technique directly leverages the richness of information present in the complex data to prevent loss of information. Specifically, this study proposes Collaborative Low-rank regularization using

both Inter and Intra-channel Correlation (CLIIC). CLIIC is founded on the observation that the matrix created by stacking vectorized slices demonstrates a low rank property owing to inherent redundancy both within and between slices, as well as within and between different channels. This low-rank characteristic stems from the presence of local consistency and shared patterns across the multi-dimensional data, enabling CLIIC to effectively exploit and leverage this redundancy for accurate and efficient MR signal restoration from heavy noise.

Suppose the size of the input MR scan is $h \times w \times n_s \times n_c \times n_r$, where $h \times w$ is the size of a slice, n_s is the number of slices in a single image, n_c is the number of channels, and n_r is the number of repetitions, including $n_r/2$ labeled images and $n_r/2$ control images. Then the complex matrix with potentially low rank $Y \in \mathbb{C}^{hw \times n_s n_c n_r}$ is formed by vectorizing each slice and stacking them together. This study aims to recover the latent noise-free image X via low-rank regularization:

$$\widetilde{X} = \arg\min_X \operatorname{rank}(X) + \frac{1}{2\lambda}\|X - Y\|_F^2 \tag{1}$$

where $\|X - Y\|_F^2$ is the data fidelity term and the regularization parameter λ controls the relative contribution of the two terms. To solve the objective function efficiently, we relax the rank penalty to the log-det of the covariance matrix [28, 29]:

$$\widetilde{X} = \arg\min_X \lambda \bullet \log|XX^*| + \frac{1}{2}\|X - Y\|_F^2 \tag{2}$$

which can be tackled through an empirical Bayesian procedure [30]. Here X^* is the conjugate transpose of X. Since λ is decided by the noise level, which can be estimate by existing techniques [31], the whole procedure does not involve any parameter tuning. After $\widetilde{X}$ is generated and coil combination is performed, the denoised ASL perfusion can be obtained by calculating the difference between the control and labeled images, and averaging across repetitions.

3. RESULTS

MRI studies were conducted on three subjects utilizing a 3T whole-body system (MAGNETOM Prisma, version MR VE11E, Siemens Healthcare, Erlangen, Germany) equipped with a 20-channel head coil. Three-dimensional (3D) pseudo-continuous arterial spin labeling (pCASL) sequence was used to generate labeled and control images. The scan parameters were TR/TE 4600/9.3 ms, fat suppression, slice thickness 2 mm, FOV 220 × 220 mm^2, matrix size 110 × 110, slice partial Fourier 5/8, 72 partitions, 6 in-plane spiral interleaves, 6 in-plane acquisition segments, partition GRAPPA 2-fold acceleration, 10 repetitions (5 labeled images and 5 control images), labeling duration 2 seconds, post label delay 1.8 seconds. Background suppression was achieved by three frequency offset

corrected inversion (FOCI) pulses. The scan time was 5 minutes and 53 seconds. The resolution of the scan was $2 \times 2 \times 2$ mm^3.

We compared denoising performance with the standard pipeline and NORDIC [32]. As shown in Fig. 1 and Fig. 2, the output of the proposed CLIIC could better reconstruct the brain patterns and more effectively remove noise. For objective quality assessment, we used a no-reference metric BRISQUE [33] because the ground truth is not available. Lower BRISQUE scores indicate better image quality. As can be seen from Fig. 3, CLIIC could decrease BRISQUE for all the slices except for the last three slices. Table 1 shows the average BRISQUE of all the slices, CLIIC improves BRISQUE by a significant margin.

4. CONCLUSIONS

This study introduced Collaborative Low-rank regularization using both Inter and Intra-channel Correlation (CLIIC), a novel approach that effectively leverages the inherent low-rank structure within multi-channel complex imaging data to enhance the quality of ASL perfusion. By preserving valuable textural information and removing noise, CLIIC significantly improved the visual quality of ASL perfusion images. Moreover, the no-reference objective metric BRISQUE demonstrated notable enhancement in image quality. The proposed technique not only avoided information loss but also eliminated the need for parameter tuning, setting it apart from previous methods.

ACKNOWLEDGMENTS

This study was supported in part by National Institutes of Health grants: R01AG060054, R01AG070227, R01EB031080-01A1, R21AG08243, R21AG080518, 5 P41EB029460-01A1, and 1UL1TR003098. Hangfan Liu is supported in part by The William H. Gates Sr. Fellowship from the AD Data Initiative.

REFERENCES

[1]. Detre JA, Leigh JS, Williams DS, and Koretsky AP, “Perfusion imaging,” Magnetic Resonance in Medicine, vol. 23, no. 1, pp. 37–45, 1992. [PubMed: 1734182]

[2]. Williams DS, Detre JA, Leigh JS, and Koretsky AP, “Magnetic resonance imaging of perfusion using spin inversion of arterial water,” Proceedings of the National Academy of Sciences, vol. 89, no. 1, pp. 212–216, 1992.

[3]. Detre JA, Wang J, Wang Z, and Rao H, “Arterial spin-labeled perfusion MRI in basic and clinical neuroscience,” Current Opinion in Neurology, vol. 22, no. 4, pp. 348–355, 2009. [PubMed: 19491678]

[4]. Fernández-Seara MA et al. , “Imaging mesial temporal lobe activation during scene encoding: comparison of fMRI using BOLD and arterial spin labeling,” Human Brain Mapping, vol. 28, no. 12, pp. 1391–1400, 2007. [PubMed: 17525983]

[5]. Chang YV, Vidorreta M, Wang Z, and Detre JA, “3D-accelerated, stack-of-spirals acquisitions and reconstruction of arterial spin labeling MRI,” Magnetic Resonance in Medicine, vol. 78, no. 4, pp. 1405–1419, 2017. [PubMed: 27813164]

[6]. Alsop DC et al. , “Recommended implementation of arterial spin-labeled perfusion MRI for clinical applications: a consensus of the ISMRM perfusion study group and the European consortium for ASL in dementia,” Magnetic Resonance in Medicine, vol. 73, no. 1, pp. 102–116, 2015. [PubMed: 24715426]

[7]. Detre JA, Rao H, Wang DJ, Chen YF, and Wang Z, “Applications of arterial spin labeled MRI in the brain,” Journal of Magnetic Resonance Imaging, vol. 35, no. 5, pp. 1026–1037, 2012. [PubMed: 22246782]

[8]. Chen Y et al. , “Quantification of cerebral blood flow as biomarker of drug effect: arterial spin labeling phMRI after a single dose of oral citalopram,” Clinical Pharmacology & Therapeutics, vol. 89, no. 2, pp. 251–258, 2011. [PubMed: 21191380]

[9]. Zheng G et al. , “Cerebral blood flow measured by arterial-spin labeling MRI: a useful biomarker for characterization of minimal hepatic encephalopathy in patients with cirrhosis,” European Journal of Radiology, vol. 82, no. 11, pp. 1981–1988, 2013. [PubMed: 23849331]

[10]. Zheng G et al. , “Changes in cerebral blood flow after transjugular intrahepatic portosystemic shunt can help predict the development of hepatic encephalopathy: an arterial spin labeling MR study,” European Journal of Radiology, vol. 81, no. 12, pp. 3851–3856, 2012. [PubMed: 22832118]

[11]. Hu W, Wang Z, Lee V-Y, Trojanowski J, Detre J, and Grossman M, “Distinct cerebral perfusion patterns in FTLD and AD,” Neurology, vol. 75, no. 10, pp. 881–888, 2010. [PubMed: 20819999]

[12]. Bibic A, Knutsson L, Ståhlberg F, and Wirestam R, “Denoising of arterial spin labeling data: wavelet-domain filtering compared with Gaussian smoothing,” Magnetic Resonance Materials in Physics, Biology and Medicine, vol. 23, pp. 125–137, 2010.

[13]. Wells JA, Thomas DL, King MD, Connelly A, Lythgoe MF, and Calamante F, “Reduction of errors in ASL cerebral perfusion and arterial transit time maps using image de-noising,” Magnetic Resonance in Medicine, vol. 64, no. 3, pp. 715–724, 2010. [PubMed: 20578044]

[14]. Wang Z, “Support vector machine learning-based cerebral blood flow quantification for arterial spin labeling MRI,” Human Brain Mapping, vol. 35, no. 7, pp. 2869–2875, 2014. [PubMed: 24443217]

[15]. Spann SM, Kazimierski KS, Aigner CS, Kraiger M, Bredies K, and Stollberger R, “Spatio-temporal TGV denoising for ASL perfusion imaging,” Neuroimage, vol. 157, pp. 81–96, 2017. [PubMed: 28559192]

[16]. Buades A, Coll B, and Morel J-M, “A non-local algorithm for image denoising,” in IEEE Conference on Computer Vision and Pattern Recognition (CVPR), 2005, vol. 2, pp. 60–65.

[17]. Liang X, Connelly A, and Calamante F, “Voxel-wise functional connectomics using arterial spin labeling functional magnetic resonance imaging: the role of denoising,” Brain Connectivity, vol. 5, no. 9, pp. 543–553, 2015. [PubMed: 26020288]

[18]. Xie D et al. , “Denoising arterial spin labeling perfusion MRI with deep machine learning,” Magnetic Resonance Imaging, vol. 68, pp. 95–105, 2020. [PubMed: 31954173]

[19]. Liu H et al., “Adaptive squeeze-and-shrink image denoising for improving deep detection of cerebral microbleeds,” in International Conference on Medical Image Computing and Computer Assisted Intervention (MICCAI), 2021: Springer, pp. 265–275.

[20]. Tao M and Yuan X, “Recovering low-rank and sparse components of matrices from incomplete and noisy observations,” SIAM Journal on Optimization, vol. 21, no. 1, pp. 57–81, 2011.

[21]. Liu H, Xiong R, Zhang J, and Gao W, “Image denoising via adaptive soft-thresholding based on non-local samples,” in IEEE/CVF Conference on Computer Vision and Pattern Recognition (CVPR), 2015, pp. 484–492.

[22]. Zhu H, Zhang J, and Wang Z, “Arterial spin labeling perfusion MRI signal denoising using robust principal component analysis,” Journal of Neuroscience Methods, vol. 295, pp. 10–19, 2018. [PubMed: 29196191]

[23]. Liu H, Xiong R, Liu D, Wu F, and Gao W, “Low rank regularization exploiting intra and inter patch correlation for image denoising,” in IEEE Visual Communications and Image Processing (VCIP), 2017, pp. 1–4.

[24]. Aharon M, Elad M, and Bruckstein A, “K-SVD: An algorithm for designing overcomplete dictionaries for sparse representation,” IEEE Transactions on Signal Processing, vol. 54, no. 11, pp. 4311–4322, 2006.

[25]. Liu H, Zhang J, and Mou C, “Image denoising based on correlation adaptive sparse modeling,” in IEEE International Conference on Acoustics, Speech and Signal Processing (ICASSP), 2021: IEEE, pp. 2060–2064.

[26]. Dabov K, Foi A, Katkovnik V, and Egiazarian K, “Image denoising by sparse 3-D transform-domain collaborative filtering,” IEEE Transactions on Image Processing, vol. 16, no. 8, pp. 2080–2095, 2007. [PubMed: 17688213]

[27]. Liu H, Xiong R, Zhang X, Zhang Y, Ma S, and Gao W, “Nonlocal gradient sparsity regularization for image restoration,” IEEE Transactions on Circuits and Systems for Video Technology, vol. 27, no. 9, pp. 1909–1921, 2016.

[28]. Mohan K and Fazel M, “Iterative reweighted algorithms for matrix rank minimization,” The Journal of Machine Learning Research, vol. 13, no. 1, pp. 3441–3473, 2012.

[29]. Liu H, Zhang X, and Xiong R, “Content-adaptive low rank regularization for image denoising,” in IEEE International Conference on Image Processing (ICIP), 2016, pp. 3091–3095.

[30]. Wipf DP, Rao BD, and Nagarajan S, “Latent variable Bayesian models for promoting sparsity,” IEEE Transactions on Information Theory, vol. 57, no. 9, pp. 6236–6255, 2011.

[31]. Coupé P, Manjón JV, Gedamu E, Arnold D, Robles M, and Collins DL, “An object-based method for Rician noise estimation in MR images,” in International Conference on Medical Image Computing and Computer-Assisted Intervention (MICCAI), 2009: Springer, pp. 601–608.

[32]. Moeller S et al. , “NOise reduction with DIstribution Corrected (NORDIC) PCA in dMRI with complex-valued parameter-free locally low-rank processing,” Neuroimage, vol. 226, p. 117539, 2021.

[33]. Mittal A, Moorthy AK, and Bovik AC, “No-reference image quality assessment in the spatial domain,” IEEE Transactions on Image Processing, vol. 21, no. 12, pp. 4695–4708, 2012. [PubMed: 22910118]

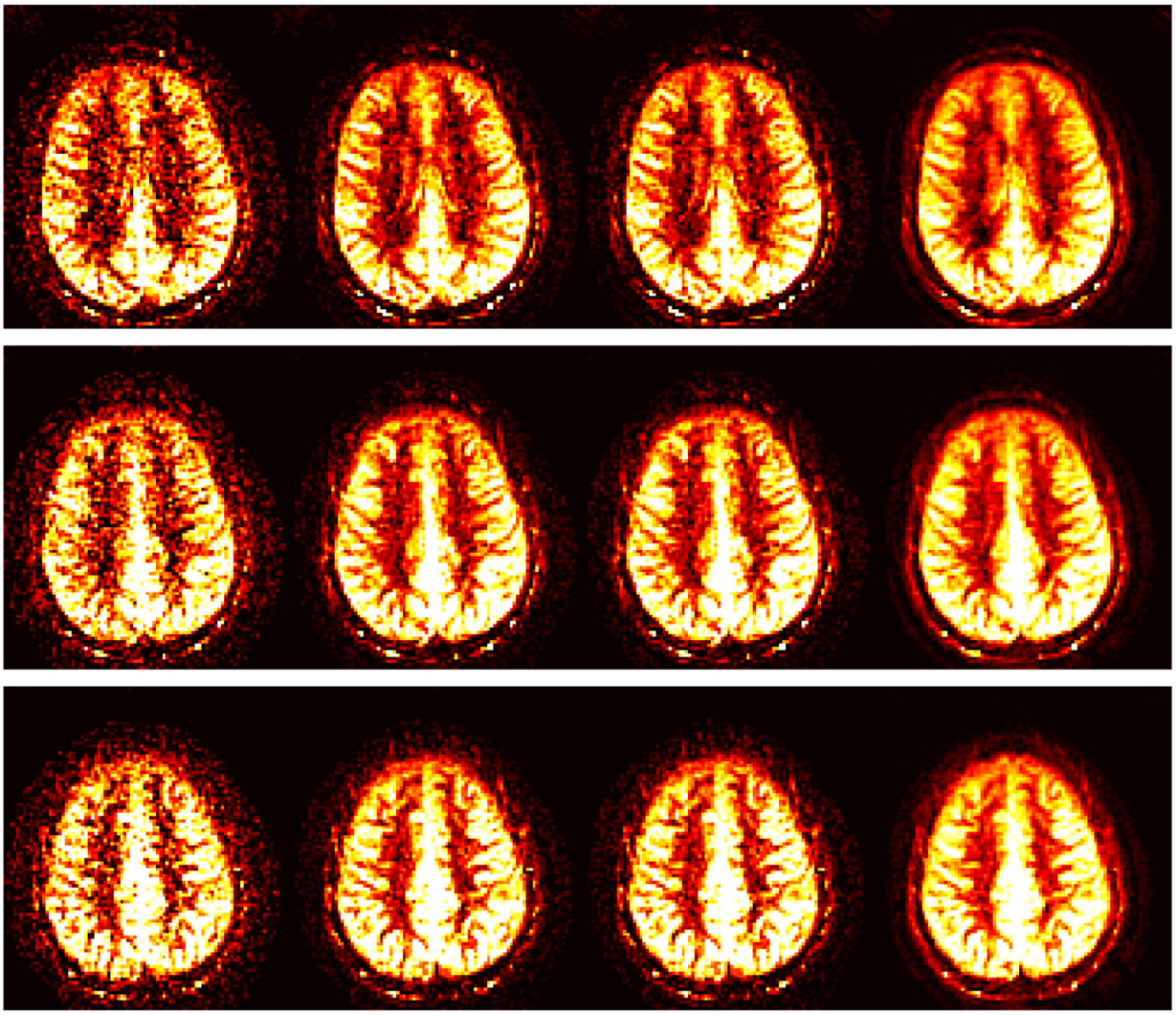

Figure 1.
Three slices of perfusion weighted images processed with different methods. Each row corresponds to one slice. (a) Raw input; (b) Standard Pipeline; (c) NORDIC; (d) CLIIC.

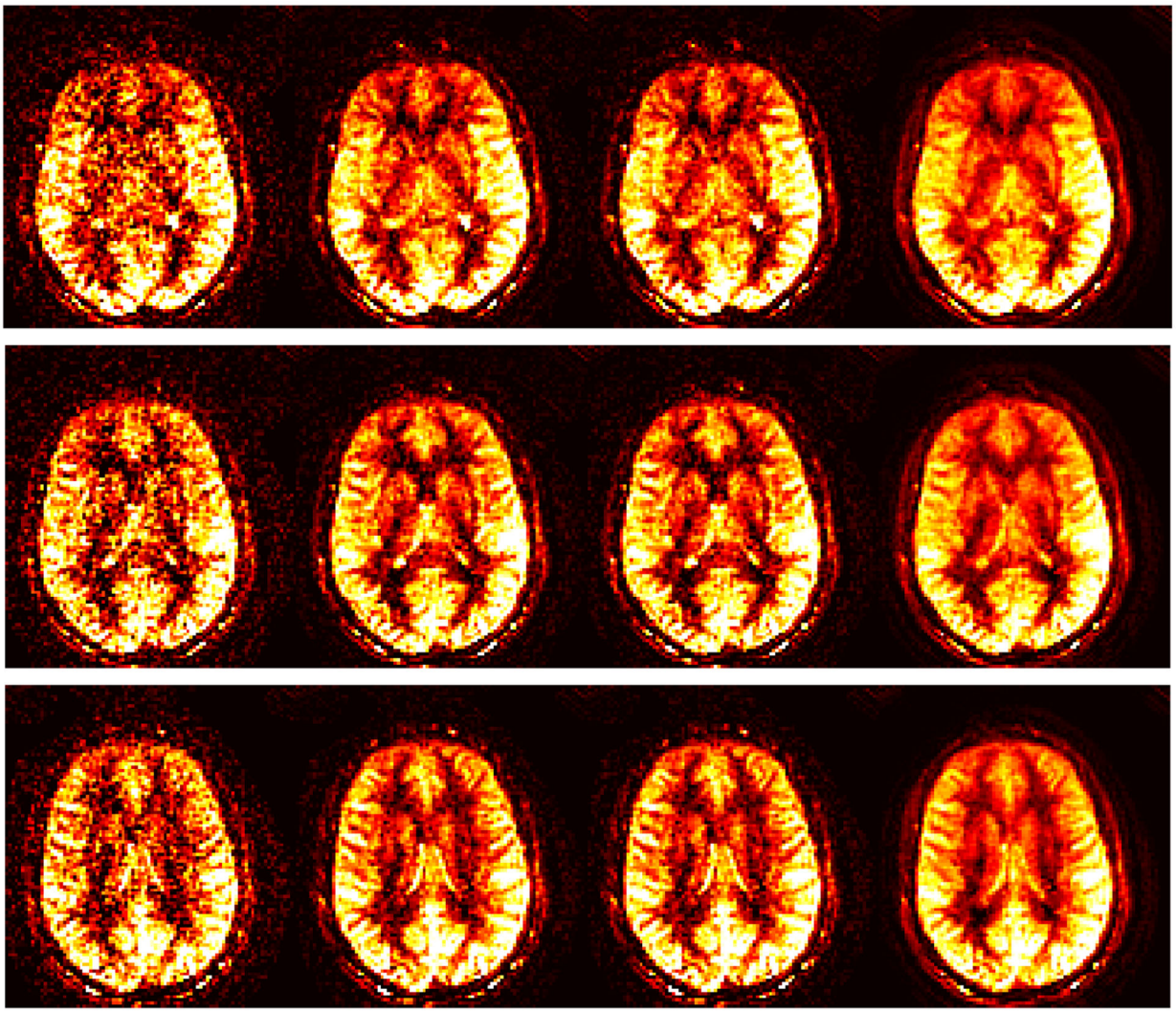

Figure 2.
Three slices of perfusion weighted images processed with different methods. Each row corresponds to one slice. (a) Raw input; (b) Standard Pipeline; (c) NORDIC; (d) CLIIC.

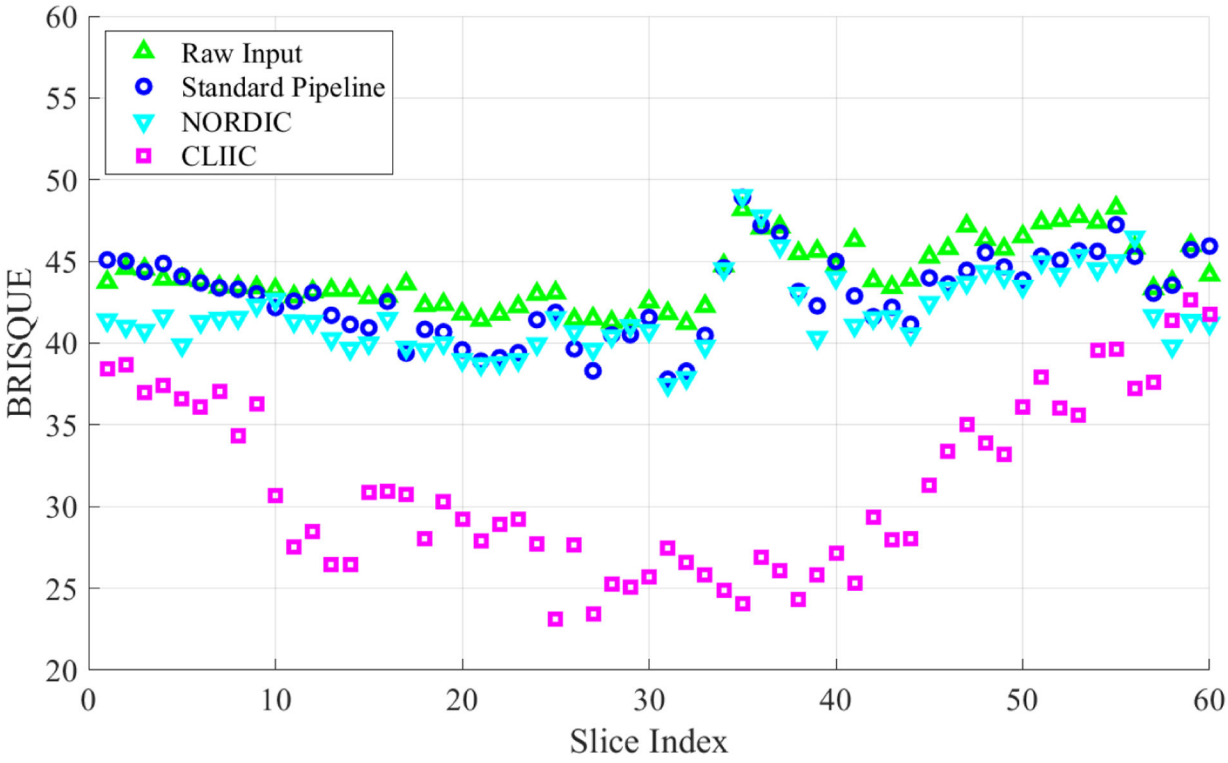

Figure 3.
Scatter plot of slice-wise BRISQUE scores.

Table 1.

Average BRISQUE of all slices. The best score is marked as **bold**.

Raw Input	Standard	NORDIC	CLIIC
44.16	42.89	41.79	**31.29**